Analysis of Long-Term Stability Uncertainty in Luminosity Measurements Using the Tile Calorimeter of the ATLAS Detector for Run 3 Proton-Proton Collisions at $\sqrt{s} = 13$ TeV in 2023

Phuti Rapheeha[1,2,3] **, Bruce Mellado**[1,2] **Karim Djouani**[3]

[1]School of Physics and Institute for Collider Particle Physics, University of the Witwatersrand, Johannesburg, Wits 2050, South Africa
[2]iThemba LABS, National Research Foundation, Somerset West 7129, South Africa
[3]School of Electrical Engineering, Tshwane University of Technology, Staatsartillerie Road, Pretoria West 0001, South Africa

E-mail: ntsoko.phuti.rapheeha@cern.ch

Abstract. Precision luminosity measurements are crucial for determining the fundamental properties of physics processes at the Large Hadron Collider. In the ATLAS experiment, luminosity uncertainties often represent one of the leading sources of systematic uncertainty in cross-section measurements, directly impacting sensitivity to new physics searches and background estimations.

Since the calibration of the primary luminometer of ATLAS, LUCID, is performed only once per data-taking year, studying the long-term stability of LUCID luminosity measurements is crucial, as it significantly contributes to the total uncertainty in the ATLAS luminosity measurement. In this study, the Tile Calorimeter is used to evaluate and monitor the long-term stability of the luminosity measurements. Results are presented for the ATLAS detector during proton-proton (pp) collisions at $\sqrt{s} = 13.6$ TeV in 2023. A long-term stability uncertainty of $\delta\mathcal{L}/\mathcal{L} = 0.1$ % is obtained for the 27.58 fb^{-1} of data delivered to ATLAS

1 Introduction

The instantaneous luminosity ($\mathcal{L}$) quantifies the rate of proton-proton (pp) collisions occurring in a collider per unit time. It plays a fundamental role in determining the expected number of events for a given physics process. The relationship between the instantaneous luminosity and the rate of observed events is given by:

$$\frac{dN_{pp\to X}}{dt} = \sigma_{pp\to X} \times \mathcal{L}, \tag{1}$$

where $dN_{pp\to X}/dt$ is the rate of events for the process $pp \to X$, and $\sigma_{pp\to X}$ is the corresponding production cross-section.

As it can be seen in Equation 1, uncertainties in the luminosity measurement directly propagate to uncertainties in cross-section measurements. For many precision measurements within the Standard Model, luminosity uncertainties are among the leading systematic uncertainties [1–4]. Searches for new physics phenomena beyond those

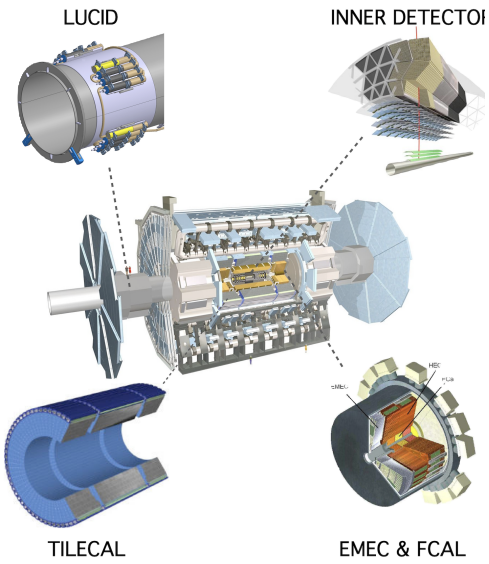

Figure 1: Illustration of some of the detectors used for luminosity measurements in the ATLAS experiment.

predicted by the Standard Model also often require accurate estimates of the luminosity to determine background levels and sensitivity.

Beyond the physics measurements, accurate and stable luminosity measurements are critical for determining trigger pre-scales and for the overall optimisation of machine operation at the LHC. For these reasons, the ATLAS experiment maintains a dedicated program for luminosity calibration and monitoring.

In the context of inelastic pp collisions at the LHC, the instantaneous luminosity per bunch crossing is related to the average number of inelastic interactions, μ, via:

$$\mathcal{L}_b = f_{\text{LHC}} \frac{\mu}{\sigma_{\text{inel}}}, \tag{2}$$

where f_{LHC} is the LHC bunch revolution frequency, and σ_{inel} is the total inelastic pp cross-section. The parameter μ represents the average number of inelastic pp interactions per bunch crossing, commonly referred to as pileup.

Alternatively, the bunch luminosity can be expressed in terms of colliding beam parameters:

$$\mathcal{L}_b = f_{\text{LHC}} \frac{n_1 n_2}{\Sigma_x \Sigma_y}, \tag{3}$$

where n_1 and n_2 are the bunch intensities, and Σ_x and Σ_y represent the beam overlap widths in the x and y planes, respectively.

Any detector sensitive to inelastic pp interactions can serve as a luminometer by measuring the visible interaction rate, μ_{vis}. For a given detector $\mu_{\text{vis}} = \epsilon\mu$, where ϵ is the efficiency of the detector to record inelastic events. The corresponding visible cross-section is defined as $\mu_{\text{vis}} = \epsilon\sigma_{\text{inel}}$.

The instantaneous bunch luminosity can also be written in terms of the visible interaction rate as:

$$\mathcal{L}_b = f_{\text{LHC}} \frac{\mu_{\text{vis}}}{\sigma_{\text{vis}}}, \tag{4}$$

This form is particularly useful for detector-based luminosity measurements, where μ_{vis} is determined from detector signals, and σ_{vis} is calibrated using dedicated beam-separation scans known as Van der Meer scans [5–7]. These scans are performed under special low-pileup conditions using low-intensity bunches that are widely spaced in time, thereby reducing the probability of overlapping events between consecutive bunch crossings.

The ATLAS experiment employs several detectors for luminosity measurements, some of which are illustrated in Figure 1. The primary luminometer is the Luminosity Cherenkov Integrating Detector (LUCID) [8], located in the forward region. Additional subsystems, including the inner tracking detectors, the Tile Calorimeter (TileCal), the endcap electromagnetic calorimeter (EMEC), and the forward calorimeter (FCal), are used to cross-check the LUCID measurement in offline analyses. More detailed information about the operating principles of the luminosity detectors employed by ATLAS can be found in Reference [9].

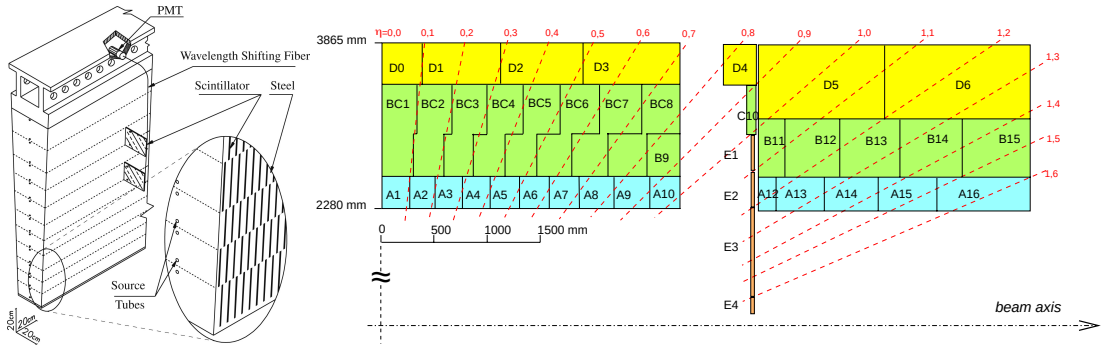

Figure 2: (*left:*) Schematic representation of a wedge-shaped TileCal module [10], illustrating the mechanical structure and optical readout components. (*right:*) Layout of TileCal cells in the ϕ–η plane on the A-side of the detector. Solid lines indicate cell boundaries, defined by grouping optical fibres from scintillating tiles for readout by photomultiplier tubes (PMTs).

LUCID is absolutely calibrated once per data-taking year during the VdM scans. Because this calibration is infrequent, it is crucial to monitor the detector's response over time to ensure the stability of the luminosity measurement. The efficiency of the luminometer may degrade due to irradiation, ageing, or other detector-specific effects, necessitating appropriate corrections. After all known corrections are applied, any residual variations are treated as systematic uncertainties related to long-term stability and linearity. In this study, the TileCal is employed as a reference luminometer to assess the time-dependent stability of LUCID throughout the 2023 pp collision data-taking period at $\sqrt{s} = 13.6$ TeV. These results contribute to the determination of the long-term stability uncertainty of the total luminosity uncertainty in ATLAS.

2 The ATLAS Tile Calorimeter

The TileCal forms the central part of the hadronic calorimeter system in the ATLAS detector. It plays a pivotal role in the reconstruction of hadrons, jets, and τ-leptons, and contributes to the measurement of missing transverse momentum associated with non-interacting particles. TileCal also provides essential information to the ATLAS trigger system.

It covers the barrel region of the ATLAS detector up to $|\eta| < 1.7$ and is segmented into three sections along the beam axis. It consists of a central Long Barrel (LB), which spans the region $|\eta| < 1.0$, and two Extended Barrels (EB), located in the forward and backward regions covering $0.8 < |\eta| < 1.7$. The detector is symmetric with respect to the interaction point: the side with positive pseudorapidity (η) is referred to as the A-side, while the side with negative η is referred to as the C-side.

The TileCal is a sampling calorimeter that uses low-carbon steel as absorber material and scintillating plastic tiles as the active medium. When a charged particle traverses the scintillating tiles, light is emitted and collected at the edges of the tiles. This light is captured by wavelength-shifting fibres, which guide it to two photomultiplier tubes (PMTs) located in a steel girder at the outer radius of each barrel module. The dual PMT readout provides redundancy and improves the signal-to-noise ratio for each cell. The PMT output is a shaped current pulse, which is read out at two amplification gains: high and low. The ratio between the high-gain and low-gain channels is 64, allowing for a wide dynamic range in signal measurement.

The readout of TileCal is divided along the beam axis into four partitions: two long barrels (LBA and LBC) and two extended barrels (EBA and EBC). Each TileCal partition consists of 64 modules with equal azimuthal width $\Delta\phi = 0.1$. The modules are oriented radially and are normal to the beam line. A schematic of a TileCal module is shown on the left in Figure 2. The ϕ, η, and radial segmentation define the three-dimensional stacks that constitute the TileCal cells within a module. The longitudinal sampling layers, denoted A, BC, and D, have a granularity of $\Delta\eta \times \Delta\phi = 0.1 \times 0.1$ in the two innermost layers and $\Delta\eta \times \Delta\phi = 0.2 \times 0.1$ in the outermost one. The cell layout of half long central barrel and extended barrel modules is shown in Figure 2 on the right.

The TileCal Technical Design Report [11] provides a detailed description of the detector, while its construction, optical instrumentation, and installation into the ATLAS detector are described in References. [12, 13].

3 Methodology

Although the TileCal was not originally designed to serve as a luminometer, the anode current, I_{PMT}, drawn by each PMT, is proportional to the number of particles traversing a given TileCal cell. As such, it is correlated with

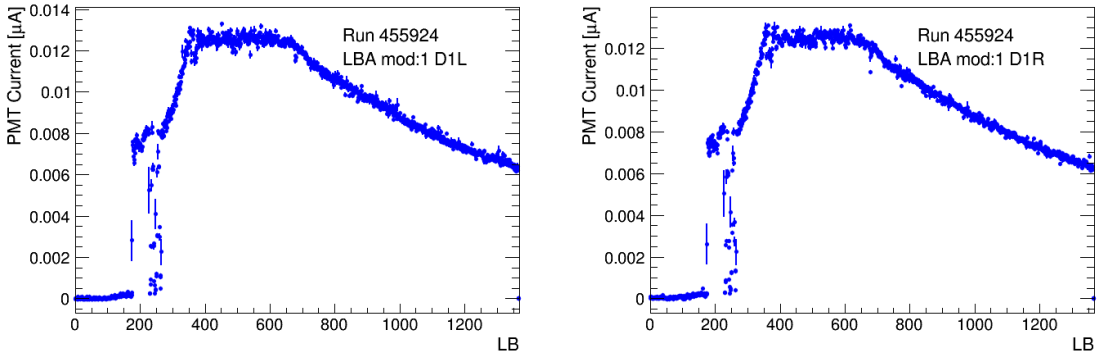

Figure 3: Distributions of raw PMT currents as a function of LB for the left (D1L, channel 13, left) and right (D1R, channel 14, right) PMTs in module 1 of the LBA partition during Run 455924.

the bunch-integrated luminosity. The anode current is derived from the raw PMT response, measured in ADC counts. It is computed as:

$$\langle I_{\mathrm{PMT}} \rangle \, [\mathrm{nA}] = \frac{\langle \mathrm{ADC} \rangle \, [\mathrm{mV}] - p \, [\mathrm{mV}]}{\text{Int. gain} \, [\mathrm{M}\Omega]}, \tag{5}$$

where $\langle \mathrm{ADC} \rangle$ represents the average ADC counts in a LB, p is the pedestal and Int. gain is the integrator gain constant. The pedestal, indicating the baseline ADC measurement primarily due to electronic noise, is calculated as the mean ADC counts before the beams are brought into collisions.

The anode currents as a function of luminosity block (LB) drawn by the left and right PMTs of cell D1 located in module 1 of the LBA partition are shown in Figure 3. An LB is a time interval, typically lasting a few seconds, during which the data-taking conditions in ATLAS are assumed to remain stable. These intervals are defined and numbered by the ATLAS central trigger processor [14], and serve as the unit of granularity for recording and reporting luminosity measurements.

The anode currents are converted to luminosity estimates using calibration constants. The relationship between the average anode current and the corresponding luminosity is given by:

$$\mathcal{L}_{\mathrm{PMT}} = \alpha \langle I\mathrm{PMT} \rangle, \tag{6}$$

where α is a calibration constant, and $\langle I_{\mathrm{PMT}} \rangle$ is the average anode current in a LB. The constants α are derived for each PMT and subsequently used to compute luminosities from PMT currents via Equation 6.

The anchoring constants used in this study are obtained from physics Run 455924, selected as the reference run for the 2023 data-taking campaign. This run features a wide luminosity range and smooth changes in instantaneous luminosity, making it ideal for deriving the calibration constants. Typically, only one run is chosen per year to determine the calibration constants, ensuring consistency across the dataset.

For each TileCal cell, the luminosity is computed as the average of the luminosities from the left and right PMTs. The luminosity of a given cell type is then determined by averaging over the corresponding cells across all modules.

In principle, all TileCal cells can be used in luminosity measurements. Cells in the D-layer, the outermost radial layer of TileCal, exhibit the most stable response over time, with minimal variation due to radiation damage. This stability makes them particularly well suited for long-term luminosity monitoring. The D6 cells are used to determine the long-term stability uncertainty, while the D5 cells serve as an additional tool for systematic cross-checks.

Figure 4 presents a comparison between the TileCal luminosities derived from the D5 and D6 cells (on both the A and C sides) and the reference track-counting luminosity. The good agreement observed across all cases demonstrates the effectiveness of the cross-calibration procedure in converting anode PMT currents into reliable TileCal luminosity measurements.

This study uses physics runs included in the standard good run list (GRL), which specifies runs and LBs deemed suitable for physics analyses. The GRL is compiled based on stringent data quality criteria, including detector performance, operational stability, and data-taking conditions. Only runs with at least 100 LBs in the GRL are considered for the long-term stability studies.

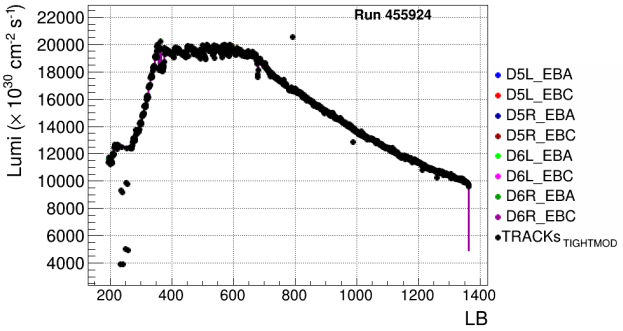

Figure 4: Comparison of TileCal luminosities derived from D5 and D6 cells with the reference track-counting luminosity. The results are shown for both the A and C sides of the detector.

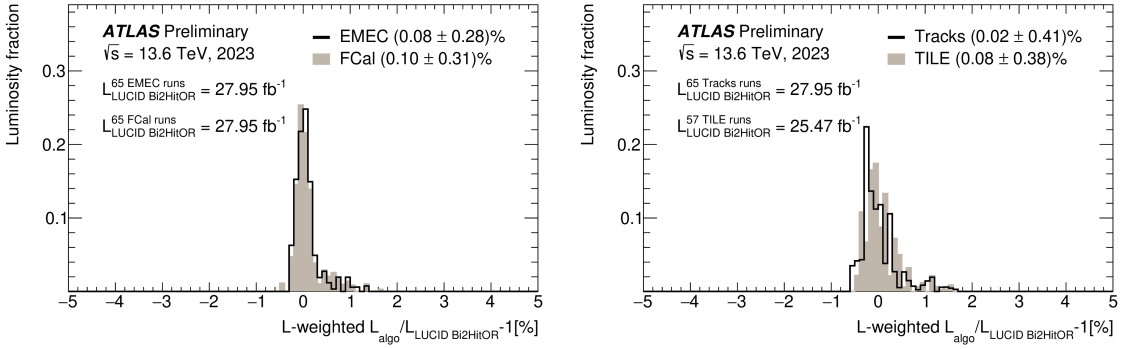

Figure 5: Distributions of the relative differences in run-integrated luminosity between the baseline LUCID measurement and (*left*) EMEC and FCal, and (*right*) TileCal and track-counting luminosity measurements, using A-side and C-side averages [15]

4 Results

Physics analyses primarily care about integrated deviation rather than per-run fluctuations. The long-term stability of LUCID luminosity measurements is evaluated by comparing the run-integrated luminosity measurements from calorimeter algorithms with those from LUCID. The long-term stability uncertainty of luminosity measurements in a data-taking year is defined as the largest measured mean deviation between LUCID and any of the calorimeter-based measurements.

Figure 5 shows the distributions of the relative differences in run-integrated luminosity between the LUCID baseline and the calorimeter and track-counting measurements. Each fill is weighted by its integrated luminosity, giving greater emphasis to longer fills with higher statistical weight. The mean and RMS values shown in the legend correspond to the average fractional deviation over the full 2023 data-taking period and its spread, respectively. The largest observed mean deviation, 0.1% from FCal, sets the preliminary long-term stability uncertainty.

5 Conclusions

Precise luminosity measurements are essential for both precision physics analyses and optimal LHC operation. This study evaluated the long-term stability of the LUCID luminosity measurement in ATLAS by comparing run-integrated luminosities to those derived from calorimeter-based and track-counting methods, with a focus on TileCal D-layer cells as a reference.

The analysis used data from the 2023 pp collision period at $\sqrt{s} = 13.6$ TeV. Calibration constants were derived from a dedicated reference run and applied consistently to convert TileCal PMT currents into luminosity estimates. Run-integrated luminosities from TileCal D6 cells and other calorimeter-based measurements were compared to the LUCID baseline measurement. The largest observed mean deviation, 0.1% from the FCal, was used to define the preliminary long-term stability uncertainty for the 2023 LUCID luminosity measurement.

References

[1] G. Aad *et al.*, "Climbing to the Top of the ATLAS 13 TeV data," *Phys. Rept.*, vol. 1116, pp. 127–183, 2025.

[2] Aad, Georges and others, "Measurement of the associated production of a top-antitop-quark pair and a Higgs boson decaying into a $b\bar{b}$ pair in pp collisions at $\sqrt{s} = 13$ TeV using the ATLAS detector at the LHC," *Eur. Phys. J. C*, vol. 85, no. 2, p. 210, 2025.

[3] G. Aad *et al.*, "Snowmass White Paper Contribution: Physics with the Phase-2 ATLAS and CMS Detectors," Geneva, 2022, all figures including auxiliary figures are available at https://atlas.web.cern.ch/Atlas/GROUPS/PHYSICS/PUBNOTES/ATL-PHYS-PUB-2022-018. [Online]. Available: https://cds.cern.ch/record/2805993

[4] Aad, Georges and others, "Measurement of the $t\bar{t}$ cross section and its ratio to the Z production cross section using pp collisions at $\sqrt{s} = 13.6$ TeV with the ATLAS detector," *Phys. Lett. B*, vol. 848, p. 138376, 2024.

[5] S. van der Meer, "Calibration of the effective beam height in the ISR," CERN, Geneva, Tech. Rep., 1968. [Online]. Available: https://cds.cern.ch/record/296752

[6] G. Aad *et al.*, "Improved luminosity determination in pp collisions at $\sqrt{s} = 7$ TeV using the ATLAS detector at the LHC," *Eur. Phys. J. C*, vol. 73, no. 8, p. 2518, 2013.

[7] C. Rubbia, "Measurement of the luminosity of $p\bar{p}$ collider with a (generalised) Van der Meer Method," CERN, Geneva, Tech. Rep., 1977. [Online]. Available: https://cds.cern.ch/record/1025746

[8] F. Lasagni Manghi, "The LUCID detector ATLAS luminosity monitor and its electronic system," *Nuclear Instruments and Methods in Physics Research Section A: Accelerators, Spectrometers, Detectors and Associated Equipment*, vol. 824, pp. 311–312, 2016, frontier Detectors for Frontier Physics: Proceedings of the 13th Pisa Meeting on Advanced Detectors. [Online]. Available: https://www.sciencedirect.com/science/article/pii/S0168900215015272

[9] Aad, Georges and others, "Luminosity determination in pp collisions at $\sqrt{s} = 13$ TeV using the ATLAS detector at the LHC," *Eur. Phys. J. C*, vol. 83, no. 10, p. 982, 2023.

[10] Aad, G. and others, "Readiness of the ATLAS Tile Calorimeter for LHC collisions," *Eur. Phys. J. C*, vol. 70, pp. 1193–1236, 2010.

[11] Abdallah, J. and others, *ATLAS tile calorimeter*, ser. Technical design report. ATLAS. Geneva: CERN, 1996. [Online]. Available: https://cds.cern.ch/record/331062

[12] J. Abdallah *et al.*, "The optical instrumentation of the ATLAS tile calorimeter," *JINST*, vol. 8, p. P01005, 2013.

[13] Abdallah, J. and others, "Mechanical construction and installation of the ATLAS tile calorimeter," *JINST*, vol. 8, p. T11001, 2013.

[14] Aad, Georges and others, "Operation of the ATLAS trigger system in Run 2," *JINST*, vol. 15, no. 10, p. P10004, 2020.

[15] "Preliminary analysis of the luminosity calibration for the ATLAS $\sqrt{s} = 13.6$ TeV data recorded in 2023," CERN, Geneva, Tech. Rep., 2024, all figures including auxiliary figures are available at https://atlas.web.cern.ch/Atlas/GROUPS/PHYSICS/PUBNOTES/ATL-DAPR-PUB-2024-001. [Online]. Available: https://cds.cern.ch/record/2900949